IEEE Access
Multidisciplinary | Rapid Review | Open Access Journal

Received December 24, 2019, accepted January 13, 2020, date of publication January 23, 2020, date of current version February 5, 2020.

Digital Object Identifier 10.1109/ACCESS.2020.2969051

Frequency Stability Support of a DFIG to Improve the Settling Frequency

JAE IK YOO[1], (Student Member, IEEE), YONG CHEOL KANG[1], (Senior Member, IEEE), EDUARD MULJADI[2], (Fellow, IEEE), KYU-HO KIM[3], (Member, IEEE), AND JUNG-WOOK PARK[1], (Senior Member, IEEE)

[1]School of Electrical and Electronic Engineering, Yonsei University, Seoul 03722, South Korea
[2]Department of Electrical and Computer Engineering, Auburn University, Auburn, AL 36849, USA
[3]Department of Electrical, Electronic and Control Engineering, Hankyong National University, Anseong 17579, South Korea

Corresponding authors: Yong Cheol Kang (yckang33@yonsei.ac.kr) and Jung-Wook Park (jungpark@yonsei.ac.kr)

This work was supported in part by the Korea Electric Power Corporation under Grant R18XA06-80, and in part by the Basic Science Research Program of the National Research Foundation of Korea (NRF) funded by the Ministry of Education under Grant NRF-2018R1D1A1B07048098.

ABSTRACT To ensure the frequency stability of a power grid, the settling frequency following a frequency event should be stabilized within the maximum steady-state frequency deviation (SSFD) band. If the frequency is stabilized at a value beyond the maximum SSFD band for high penetrations of variable renewable energy, the frequency cannot be restored to the nominal frequency because automatic generation cannot be activated. This paper proposes a primary frequency control support scheme of a doubly-fed induction generator (DFIG) to improve the settling frequency following an event. In the proposed scheme, if the frequency following an event is stabilized at a value beyond the maximum SSFD band, to reduce the output power of synchronous generators, the output power of a DFIG is instantly increased by a constant and maintained until the frequency increases to within the maximum SSFD band. At the same time, the mechanical input power of the synchronous generators is maintained so that the difference between the mechanical input power and electrical output power of the synchronous generators increases the frequency to a value within the maximum SSFD band. The simulation results demonstrate that the proposed scheme can improve the settling frequency while avoiding additional system defense plans when the settling frequency is stabilized at a value beyond the maximum SSFD band.

INDEX TERMS Frequency stabilization, settling frequency, doubly-fed induction generator, high penetration of VRE, synchronous generator.

I. INTRODUCTION

To ensure the stable operation of an electric power grid, the frequency should be maintained within a certain range following an event. When a frequency event occurs, kinetic energy is intrinsically released from the synchronous generators as an inertial response; then, the frequency keeps decreasing until the power imbalance between generation and load vanishes [1]. If the frequency decreases beyond the governor deadband of the synchronous generators, primary frequency control (PFC) is activated to arrest the frequency decline. The frequency decline is arrested when the imbalance between generation and load vanishes; the arrested frequency is called the frequency nadir (f_{nadir}). Afterward, the frequency rebounds and is stabilized; this is called the settling frequency (f_{set}). f_{set}, however, is less than the nominal value (f_0) because PFC is based on proportional control [2]. To restore f_{set} to f_0, a secondary frequency control (SFC) scheme, automatic generation control (AGC), is activated.

For a power grid that has high penetrations of variable renewable energy (VRE) such as wind and solar energy, the frequency stability can be jeopardized if VRE maintains maximum power point tracking (MPPT) operation following an event [3]–[6]. This is because f_{nadir} and/or f_{set} are lowered. To ensure the frequency stability for high penetrations of VRE, both f_{nadir} and f_{set} should be improved.

To improve f_{nadir}, a number of synthetic inertia control (SIC) schemes of a variable-speed wind turbine generator (WTG) have been reported in the literature [7]–[15].

The associate editor coordinating the review of this manuscript and approving it for publication was Ying Xu.

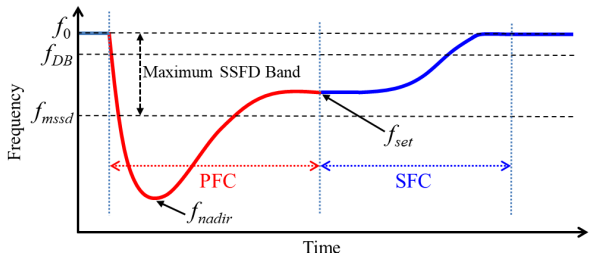

FIGURE 1. PFC and SFC following an event.

Prior to an event, a variable-speed WTG performs MPPT operation. When an event occurs, SIC schemes temporarily release the kinetic energy stored in the rotating masses in a WTG to improve f_{nadir}. Schemes relying on the measured system frequency were reported in [7]–[12]; these schemes provide a slow response. To achieve a rapid response, the authors of [13]–[15] suggested fast SIC that instantly increase the output power upon detecting an event.

SIC schemes are able to improve f_{nadir} but not f_{set}. For high penetrations of VRE, if the frequency is stabilized at a value beyond the maximum steady-state frequency deviation (SSFD) band, the frequency cannot be restored to f_0 because AGC cannot be activated [16]. In this case, to increase f_{set} to a value that is more than f_{mssd}, which is defined as f_0 minus the maximum SSFD in this paper, additional system defense plans should be activated, such as quick-starting generators and interruptible loads [1], but these require additional operating costs. Little attention has been paid to improve f_{set} even though f_{set} should also be improved for ensuring the frequency stability in a power grid that has high penetrations of VRE.

This paper proposes a PFC support scheme of a doubly-fed induction generator (DFIG) that can improve f_{set} in association with the control of synchronous generators. In the proposed scheme, if the frequency following an event is stabilized at a value less than f_{mssd}, to improve the frequency, a DFIG instantly increases its output power by a constant and maintains it until the frequency increases to a value more than f_{mssd}. During this period, the mechanical input power of the synchronous generators is maintained so that the difference between the mechanical input power and electrical output power of the synchronous generators forces the frequency to increase to a value that more than f_{mssd}, thereby enabling AGC to restore the frequency to f_0. The efficacy of the proposed scheme is verified under various wind speeds and wind penetration levels in the IEEE 14-bus system based on an EMTP-RV simulator.

II. PRIMARY AND SECONDARY FREQUENCY CONTROL IN A POWER GRID

This section briefly describes the basic principles of PFC and SFC in a power grid to provide the theoretical background of the proposed PFC support scheme.

Fig. 1 illustrates the frequency response following an event. If an event occurs, to arrest and stabilize the declining frequency, the online synchronous generators participating in PFC autonomously release PFC reserve based on the droop characteristics of the governor [17]. As a result, the frequency is stabilized at f_{set}, which is a value less than f_0. To restore f_{set} to f_0, the transmission system operator activates AGC, allowing the synchronous generators participating in SFC to release SFC reserve.

To describe the behavior of the system frequency ($\omega = 2\pi f$), the swing equation of an overall power grid neglecting losses can be represented as:

$$J\omega_0 \frac{d\omega}{dt} = P_m - P_e \tag{1}$$

where J is the total inertia of the system, and ω_0 is the nominal frequency; and P_m and P_e are the total mechanical input power and total electrical output power of all synchronous generators in a power grid, respectively.

Prior to an event, the mismatch between P_m and P_e, which is generally caused by the load variation, is small, and thus the frequency deviation is relatively small. In this stage, the frequency can be maintained within a narrow band through frequency regulation schemes in a power grid, which is operated in association with AGC.

At the instant of an event, the significant mismatch between P_m and P_e corresponding to the output power of the tripped generator is applied to the synchronous generators, thereby starting the frequency decline. When the frequency deviation exceeds the governor deadband of synchronous generators (f_{DB}), each synchronous generator participating in PFC starts increasing P_m based on its droop characteristics. As time goes on, $d\omega/dt$ decreases because P_m gradually increases with increases in the frequency deviation. The frequency decline is arrested at f_{nadir} when the mismatch between P_m and P_e vanishes. During this stage, if the frequency decreases to a value less than f_{mssd}, AGC is disabled. Afterward, the frequency rebounds and is stabilized at f_{set}. Note that f_{set} cannot be restored to f_0 by PFC action only because the proportional control used for PFC intrinsically causes a steady-state error. Thus, f_{set} should be more than f_{mssd} so that AGC is reactivated to restore the frequency to f_0. Otherwise, the frequency cannot be restored to f_0, and thus additional system defense plans are required, such as quick-starting generators and interruptible loads to increase f_{set} to more than f_{mssd}.

Fig. 2 illustrates the simplified power-frequency (P_m-f) characteristic of an overall power grid while performing PFC. The slope between (f_{mssd}, P_{m1}) and (f_{DB}, P_{m0}), which is called the frequency response (β) in MW/0.1 Hz [17], can be obtained from the P_m-f characteristic of each synchronous generator participating in PFC by using:

$$\beta = \sum_i \frac{100}{R_i} \frac{S_i}{f_0} \frac{1}{10} \ (MW/0.1Hz) \tag{2}$$

where R_i and S_i are the droop coefficient in percentage and installed capacity of the i-th synchronous generator participating in PFC, respectively.

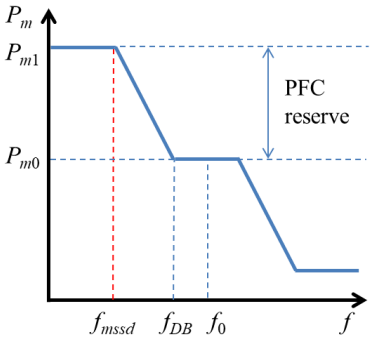

FIGURE 2. P_m-f characteristic for PFC in an overall power grid.

Note that β depends on the number, capacity, and R_i of the synchronous generators participating in PFC. In addition, the amount of PFC reserve is set to be the size of the reference event in the corresponding power grid. Thus, if the reference incident occurs and PFC reserve is fully deployed, the frequency is stabilized at f_{mssd}. Thus, as a result of PFC, the frequency is generally stabilized at a value between f_{DB} and f_{mssd} because the size of an event is less than the reference incident. If load damping is considered following an event, f_{set} becomes more than it is when the load remains the same after an event.

For high penetrations of VRE, β and/or PFC reserve might decrease if the number of generators participating in PFC decreases and/or PFC reserve from VRE is not fully deployed. In this case, f_{set} is stabilized at a value that is less than f_{mssd} depending on the decrease in β and deployed PFC reserve. This results in activating the additional system defense plan, thereby increasing operating costs.

III. PROPOSED PFC SUPPORT SCHEME TO IMPROVE THE SETTLING FREQUENCY

The proposed PFC support scheme aims to increase f_{set} to a value that is more than f_{mssd} while avoiding additional system defense plans if f_{set} is stabilized at a value less than f_{mssd}. When the frequency is stabilized, $d\omega/dt$ equals zero; this means that P_m equals P_e. Thus, to increase f_{set} to more than f_{mssd}, the differential power between P_m and P_e should be applied to synchronous generators (refer to (1)).

In this paper, to obtain the differential power that should be applied to the synchronous generators, a DFIG instantly increases its output power by a constant (ΔP) and maintains it until f_{set} increases to more than f_{mssd}, which is denoted as ΔT in Fig.3(a). Fig. 3(b) illustrates the dynamic behavior of ω_r while performing the proposed control scheme. Until the frequency is stabilized ($t < t_0$), P_{ref} in the proposed scheme equals P_{MPPT}. As soon as the frequency is stabilized or a command signal for activation is received from a power grid operator, P_{ref} instantly increases ΔP and this value is maintained during the period of ΔT (see Fig. 3(a)). This indicates that the operating point of a WTG moves upward from Point A to Point B in Fig. 3(b). From t_0 to $t_0 + \Delta T$,

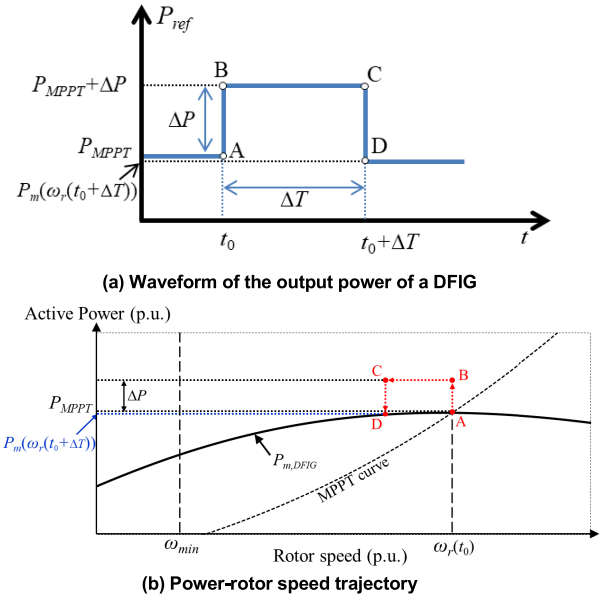

FIGURE 3. Operational characteristics of a DFIG for increasing f_{set}.

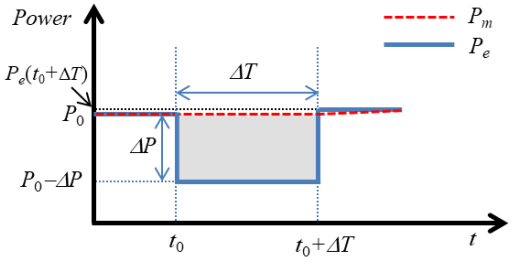

FIGURE 4. P_m and P_e of synchronous generators.

the electrical output power of a WTG is larger than the mechanical input power and thus ω_r keeps decreasing until it reaches Point C. At Point C, P_{ref} instantly decreases from Point C to Point D, where the electrical output power of a WTG is the same as the mechanical input power of a WTG ($P_m(\omega_r(t_0 + \Delta T))$); thus, ω_r stops decreasing. Note that P_{ref} at Point D is slightly smaller than P_{ref} at Point A. ΔP and ΔT in Fig. 3 can be determined depending on J. Thus, a DFIG can release part of the kinetic energy stored in the rotating masses to improve f_{set}.

As a result of the increase in the output power of a DFIG, the value of P_e instantly decreases from P_0 to $P_0 - \Delta P$ to meet the total load (see P_e in Fig. 4). From t_0 to $t_0 + \Delta T$, the differential power between P_m and P_e keeps increasing the frequency. At $t = t_0 + \Delta T$, P_e instantly increases from $P_0 - \Delta P$ to $P_e(t_0 + \Delta T)$, which is slightly larger than P_0.

P_m consists of the output signal of the governor (P_{gov}) and the output signal of AGC (P_{AGC}) as in (see Fig. 5):

$$P_m = P_{gov} + P_{AGC} \tag{3}$$

As the frequency increases, the frequency deviation decreases, thereby decreasing P_{gov}. As a result, P_m decreases until P_m reaches P_e. In this case, the frequency stops increasing. To avoid this, in the proposed scheme, P_{gov} is maintained

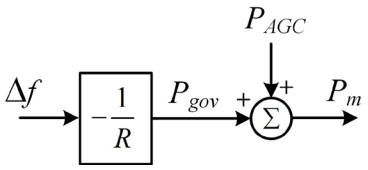

FIGURE 5. Relationship between P_m and P_{gov}.

during ΔT to maintain P_m (see P_m in Fig. 4). The shaded area between P_m and P_e in Fig. 4—which indicates the energy transferred from a DFIG to the synchronous generators—increases the frequency to more than f_{mssd}. Thus, AGC can be activated to restore the frequency to f_0.

There are several ways to determine ΔP and ΔT in Fig. 3. If these parameters are set to a fixed value, difficulties arise in selecting them suitable for various penetration levels and event sizes. Thus, to take account of the total inertia of a power grid (J), which varies with the penetration level of VRE, ΔP is determined from (1) so that the increase rate of frequency becomes 20 mHz/s, which is set based on the various simulation results in the model system. Special attention should be paid to select ΔP; a large value of ΔP causes the frequency fluctuation after disabling the proposed scheme, whereas a small value of ΔP delays the frequency restoration to f_0. In addition, to select ΔT suitable for various system and event conditions, the proposed scheme applies ΔP until the frequency reaches a target frequency, which is higher than f_{mssd} and is set to 59.6 Hz in this paper. In other words, the proposed scheme selects the target frequency instead of ΔT. The target frequency is set based on the various simulation results in the model system as in ΔP. A high value of the target frequency can cause the severe frequency fluctuation after disabling the proposed scheme, whereas a small value of the target frequency can decrease the frequency again to a value smaller than f_{mssd} after the proposed scheme is disabled, thereby delaying the frequency restoration to f_0.

In power grids with higher penetrations of wind, f_{set} can be much less than f_{mssd}. Thus, we can assume that each WTG should release a large amount of kinetic energy to increase f_{set}, thereby causing overdeceleration. However, for a higher penetration of WTGs, because the required kinetic energy to increase f_{set} can be shared by all WTGs to a power grid, each WTG can release less kinetic energy, thereby preventing overdeceleration. Therefore, the proposed scheme can perform even better with a larger amount of kinetic energy.

IV. DFIG-BASED WIND TURBINE GENERATOR

Fig. 6(a) shows the configuration of a DFIG, which includes a wind turbine, gearbox, induction generator, back-to-back converters, and control system. To represent the mechanical dynamics of the wind turbine and generator, a two-mass-shaft model is used, as in [18]. The fifth-order model with voltage and flux equations in the dq synchronous reference frame is used for the induction generator.

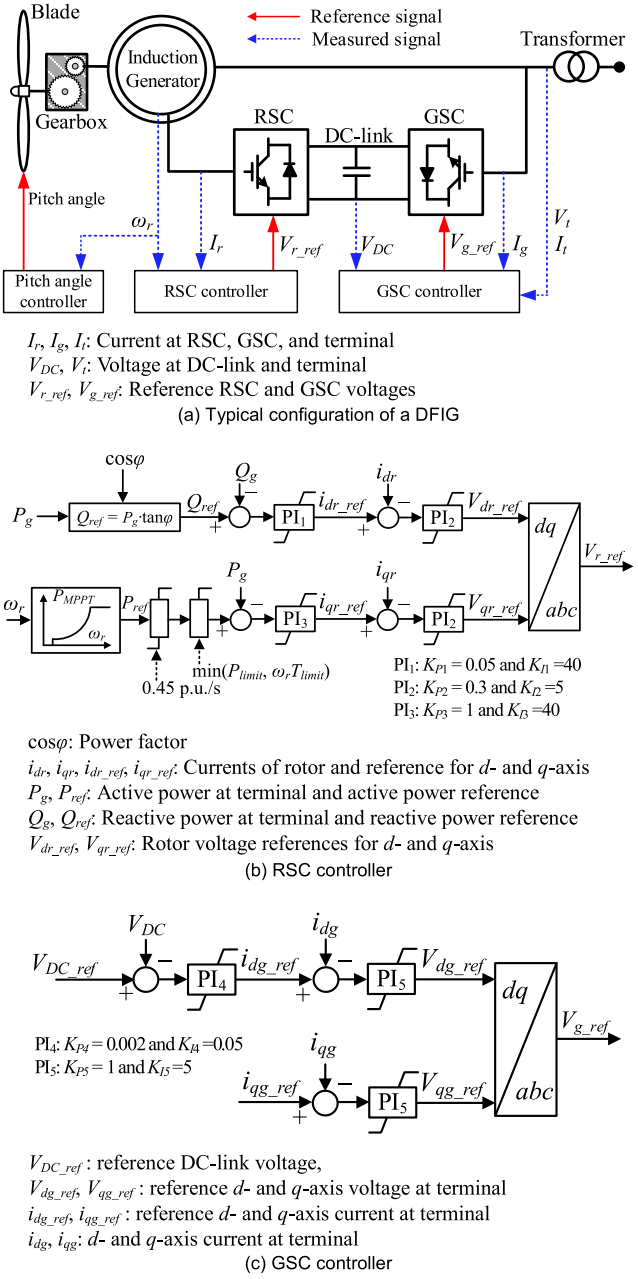

FIGURE 6. Configuration and controllers of the DFIG model.

The DFIG control system consists of a rotor-side converter (RSC) controller, grid-side converter (GSC) controller, and pitch-angle controller. An RSC controls the active power and reactive power supplied to a power grid; the active power control loop includes the MPPT control loop (see Fig 6(b)).

The reference for MPPT operation (P_{MPPT}) is represented by (4), as in [19]:

$$P_{MPPT} = k_g \omega_r^3 \tag{4}$$

where k_g is set to 0.512 in this paper, and ω_r is the rotor speed of the DFIG.

A GSC controls the DC-link voltage and requested reactive power, as shown in Fig. 6(c). In addition, to prevent ω_r from

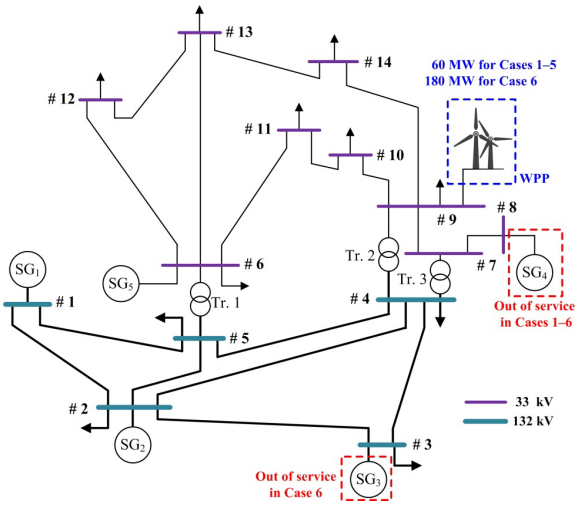

FIGURE 7. Modified IEEE 14-bus system with a DFIG-based WPP.

TABLE 1. Parameters of the synchronous generators in the IEEE 14-Bus system.

Synchronous Generator	SG_1	SG_2	SG_3	SG_4	SG_5
Apparent Power (MVA)	120	120	110	80	70
Inertia Constant (s)	4	4	4	3	3

exceeding the maximum ω_r operating limit, a pitch-angle controller is used.

The cut-in, cut-out, rated wind speeds are 4 m/s, 25 m/s, and 11 m/s, respectively. The stable operating range of ω_r is from 0.70 p.u. to 1.25 p.u.

V. CASE STUDIES

The modified IEEE 14-bus system is used to verify the performance of the proposed frequency stability support scheme of a DFIG using an EMTP-RV simulator, as shown in Fig. 7 and Table 1. The original IEEE 14-bus system includes five synchronous generators, whereas the modified IEEE 14-bus system includes three or four synchronous generators and one aggregated DFIG-based wind power plant (WPP) to reflect the high penetration level of VRE. Buses 1 to 5 are 132 kV, and buses 6 to 14 are 33 kV. In addition, the model system includes eleven loads, and the total load is set to 297 MW and 75 MVAr.

All synchronous generators in the model system are assumed to be steam turbine generators that use the IEEEG1 steam governor model with a tandem-compound, single-reheat turbine [20]. Fig. 8 and Table 2 show the IEEEG1 steam governor model and its parameters, respectively. The droop setting in the governor response was set to 3.33%, and thus β in the original IEEE 14-bus system is set to 25 MW/0.1 Hz. The reference incident is set to 120 MW, which is the capacity of the largest synchronous generator (SG_1) in the model system. The deadband of the governor for the synchronous generators is set to 20 mHz and fmssd is set to 59.5 Hz.

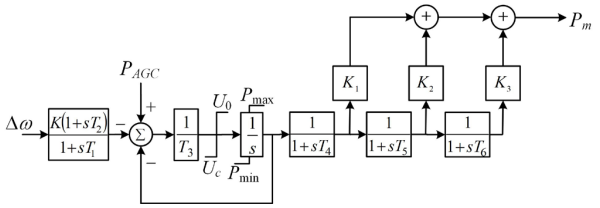

FIGURE 8. IEEEG1 steam governor model (tandem-compound, single-reheat).

TABLE 2. Parameters of the IEEEG1 steam governor model.

K	K_1	K_2	K_3	T_1	T_2	T_3
30	0.3	0.4	0.3	0.1	1.0	0.25
T_4	T_5	T_6	U_o	U_c	P_{max}	P_{min}
0.3	10	0.4	0.3	–0.3	1.5	0.4

TABLE 3. Initial load consumptions at the buses.

Bus Number	P_0 (MW)	Q_0 (MVAr)	Bus Number	P_0 (MW)	Q_0 (MVAr)
1	-	-	8	-	-
2	84.09	12.7	9	34.20	7.5
3	51.25	19.0	10	10.44	5.8
4	40.93	–2.1	11	4.06	1.8
5	23.30	1.6	12	7.07	1.6
6	12.99	16.6	13	15.65	5.8
7	-	-	14	12.28	5.0

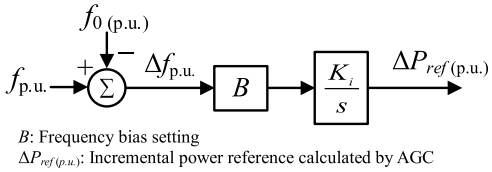

FIGURE 9. Functional diagram of AGC.

In this paper, the voltage-dependent constant impedance model is used for the loads at the buses, and Table 3 shows the initial load consumptions at the buses.

Fig. 9 shows the functional diagram of AGC used in the model system, as in [21]. To remove the frequency error, $\Delta f_{p.u.}$ is passed through an integral controller. Afterward, $\Delta P_{ref\,(p.u.)}$ is distributed to individual synchronous generators every 4 s. B and K_i are set to 20 and 0.0168, respectively, which are the settings in Korea's power grid.

The performance of the proposed PFC support scheme is investigated under the scenarios by varying wind speed, size of an event, and wind penetration level. The wind penetration level in this paper is defined as the installed capacity of a WPP divided by the total load [22]. As a frequency event, SG_2 is tripped at 10.0s.

Table 4 shows the output power of the synchronous generators and the WPP for all cases prior to an event. For Cases 1–5, SG_4 is replaced by the WPP of 60 MW; for Case 6, SG_3 and SG_4 are replaced by the WPP of 180 MW. Table 5 shows ΔP in the proposed scheme obtained from (1). In all cases in this paper, the proposed scheme is activated 60 s after an event to provide the clear comparison results between the cases;

TABLE 4. Output power of SGs and the WPP for all cases prior to an event.

Case	Load (MW)	SG_1 (MW)	SG_2 (MW)	SG_3 (MW)	SG_4 (MW)	SG_5 (MW)	WPP (MW)
1	288.9	67.3	90.0	66.8	-	42.6	32.0
2	287.2	73.1	90.0	72.2	-	46.0	15.1
3	287.1	73.9	90.0	71.6		45.7	15.1
4	287.2	69.1	100.0	68.5	-	43.6	15.1
5	287.2	65.0	110.0	64.9	-	41.3	15.1
6	276.6	84.0	110.0	-	-	50.5	45.3

TABLE 5. ΔP in the proposed scheme for all cases.

Case	Proposed Scheme (p.u.)	Wind Penetration Level (%)
1	0.0125	20
2	0.0125	20
3	0.0125	20
4	0.0125	20
5	0.0125	20
6	0.0022	60

however, the proposed scheme can be alternatively activated when the frequency is stabilized.

A. EFFECTS OF WIND SPEEDS

The performance of the proposed scheme can be affected by the stored energy in a DFIG, which corresponds to the wind speed. This is because the proposed scheme releases the stored kinetic energy from a DFIG. Thus, this subsection describes the investigation results for wind speeds of 9 m/s and 7 m/s.

1) CASE 1: WIND PENETRATION LEVEL = 20%, WIND SPEED = 9 m/s, AND SG_2 TRIP = 90 MW

Fig. 10 shows the results for Case 1. For 'w/o WPP' in Fig. 10, which means the results in the original IEEE 14-bus system, the frequency is stabilized at 59.562 Hz 15.8 s after an event and then is restoring to f_0. However, for MPPT operation, the frequency is stabilized at 59.475 Hz at 22.1 s after an event; this value is maintained because AGC is not activated. The reason for this is as follows. If β and the load consumption are unchanged after the event, f_{set} is expected to be 59.620 Hz, which is obtained as 60.0 – 90·0.1/25 – 0.02 Hz. After the event, however, β is changed from 25 MW/0.1 Hz to 15 MW/0.1 Hz because SG_2 is tripped and SG_4 is out of service (see Table 4). In addition, the load consumption is reduced from 288.9 MW to 274.0 MW. Thus, f_{set} is further reduced to 59.475 Hz.

The proposed scheme starts at 70.0 s. The DFIG instantly increases its output power by 0.750 MW at 70.0 s. As a result, P_e decreases by 0.750 MW to meet the load. To apply the constant differential power to the synchronous generators, P_{gov} is maintained so that P_m is also maintained. Thus, the differential power increases the frequency at a rate of 20 mHz/s because ΔP of a DFIG is set to 0.0125 p.u. Note that in Fig. 10(d) the difference between P_m and P_e prior to the event is the power loss. At 76.0 s, when the frequency reaches 59.6 Hz (target frequency), the DFIG instantly reduces its output to the original value. During the interval from 70.0 s to76.0 s, the DFIG releases part of the stored energy, and thus the rotor speed decreases from 1.014 p.u. to 1.006 p.u. (see Fig. 10(e)).

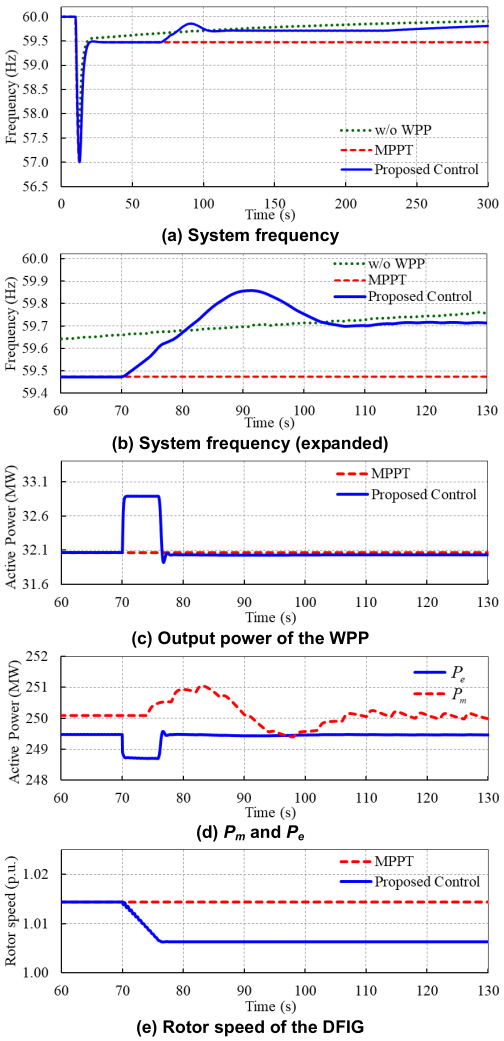

FIGURE 10. Results for Case 1.

Although the value of P_{gov} is maintained from 70.0 s to 76.0 s, P_m increases from 74.0 s because of the AGC activation. In addition, at 76.0 s, P_{gov} might decrease because of the increase in the frequency, thereby reducing P_m. In this case, the frequency might decrease again to less than f_{mssd} unless there is enough time for AGC to increase the frequency. Thus, in the proposed scheme P_{gov} is smoothly returned to the original P_{gov} (see Fig. 10(d)).

The proposed scheme operates for 156.0 s. From 226.0 s, only AGC action gradually increases the frequency to f_0. From 74.0 s, P_m fluctuates because of the dynamic response of the steam turbine; in addition, ripples are shown in P_m because P_{AGC}, which is issued every 4 s, is maintained for 4 s.

2) CASE 2: WIND PENETRATION LEVEL = 20%, WIND SPEED = 7 m/s, AND SG_2 TRIP = 90 MW

Fig. 11 shows the results for Case 2. The output power of the WPP decreases, whereas the output powers of the

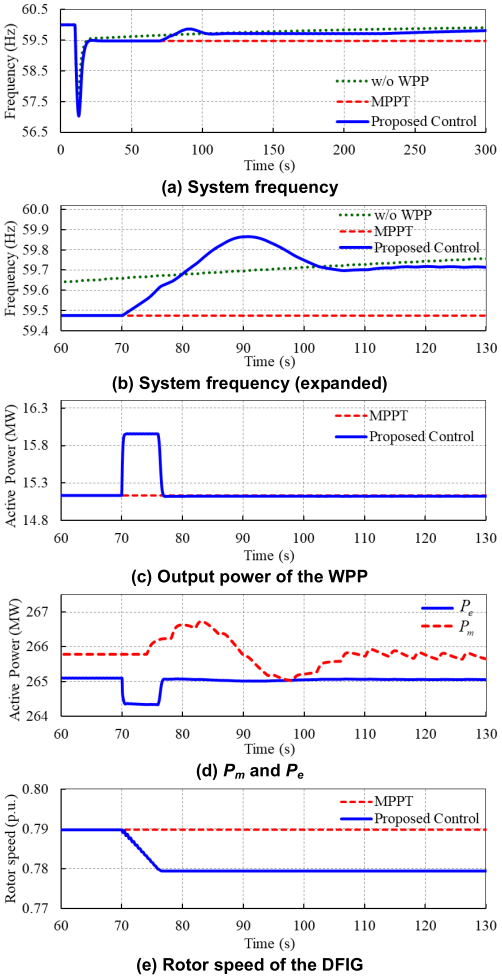

FIGURE 11. Results for Case 2.

synchronous generators increase (see Table 4). After the event, β is 15 MW/0.1 Hz, as in Case 1, because the number and capacity of the synchronous generators are the same. The load consumption is changed from 287.2 MW to 272.0 MW. As a result, f_{set} is 59. 477 Hz, which is similar to that in Case 1. The output power of DFIG is instantly increased by 0.750 MW at 70.0 s, as in Case 1; thus, P_e is reduced by 0.750 MW, and P_{gov} is maintained. The output power of the DFIG returns to its original value at 76.0 s. As a result, the frequency successfully increases to more than f_{mssd} so that AGC is activated.

The releasable energy of the DFIG in Case 1 and Case 2 are 2.695 s and 0.669 s, respectively. The proposed scheme releases 0.081 s in Case 1 and 0.080 s in Case 2, which is 3.0% and 12.0% of the releasable energy, respectively. The results in Cases 1 and 2 indicate that the proposed scheme can improve the settling frequency to more than the f_{mssd} in various wind speeds without additional system defense plans.

B. EFFECTS OF VARYING WIND SPEEDS

Continuously varying wind speeds can affect the proposed control because it changes the stored kinetic energy and output power of the DFIG. Thus, this subsection describes

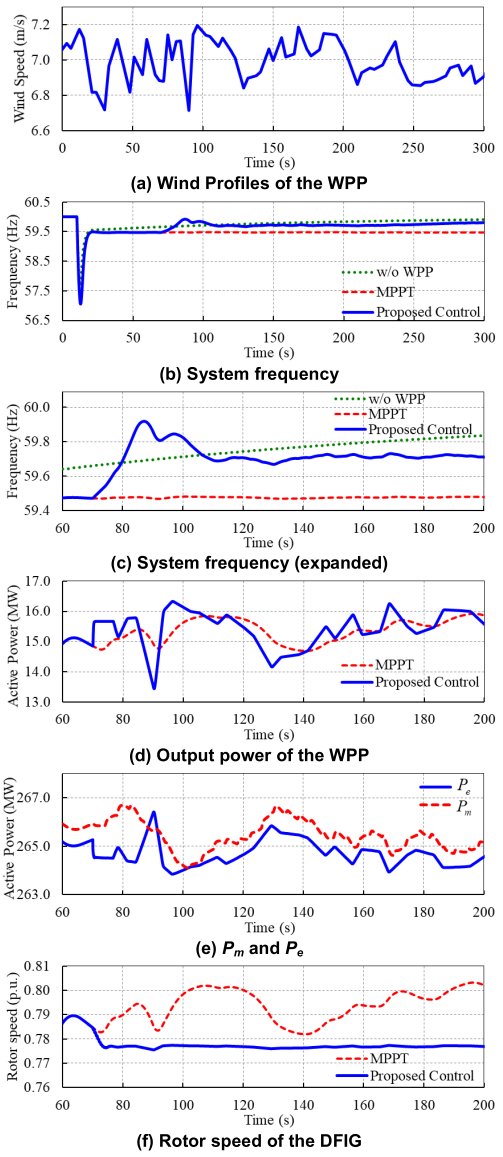

FIGURE 12. Results for Case 3.

the investigation results for continuously varying wind speeds with the average wind speed of 7 m/s.

1) CASE 3: WIND PENETRATION LEVEL = 20%, CONTINUOUSLY VARYING WIND SPEED, AND SG_2 TRIP = 90 MW

Fig. 12 shows the results for Case 3, in which the average wind speed is the same as in Case 2. After the event, β in Case 3 is 15 MW/0.1 Hz. The load consumption is changed from 287.1 MW to 271.7 MW. As a result, f_{set} is 59.473 Hz, which is similar to that in Case 2. The output power of the DFIG is instantly increased by 0.750 MW at 70.0 s, as in Case 2 (see Fig. 12(d)); thus, P_e is reduced by 0.750 MW, and P_{gov} is maintained (see Fig. 12(e)). The output power of the DFIG returns to its original value at 76.2 s. In this case, although the system frequency fluctuates more severely than it does in Case 2 after disabling the proposed scheme, the frequency successfully increases to more than f_{mssd} so

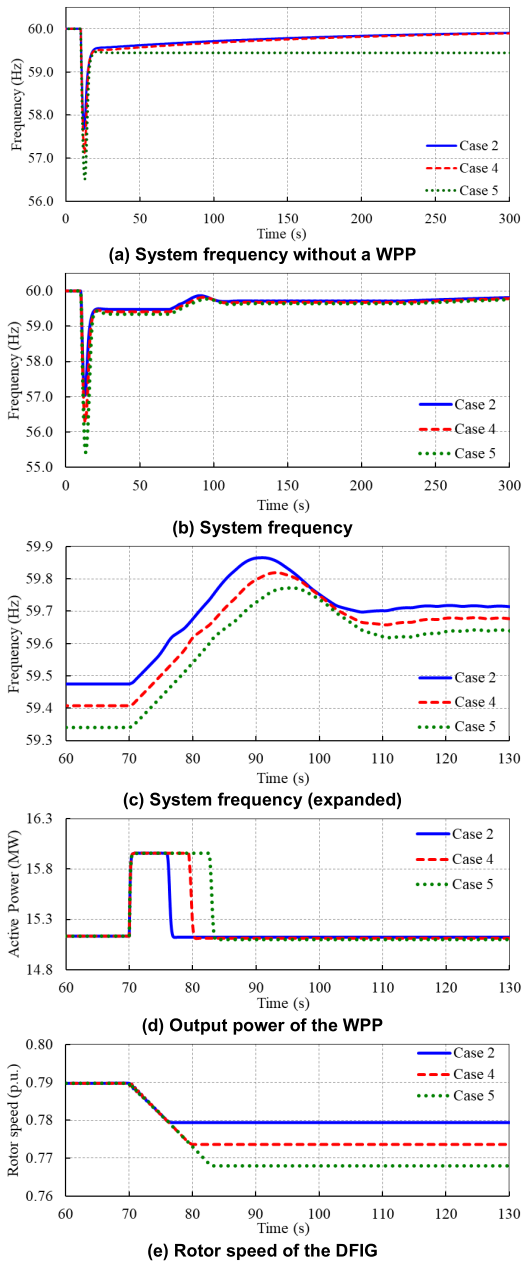

FIGURE 13. Results for Case 4 and Case 5.

that AGC is activated (see Figs. 12(b) and 12(c)). During this interval, the rotor speed decreases from 0.785 p.u. to 0.776 p.u. (see Fig.12(f)).

C. EFFECTS OF SIZES OF EVENT

The settling frequency depends on the size of an event. Thus, this subsection describes the investigation results for events of 100 MW and 110 MW.

1) CASE 4: WIND PENETRATION LEVEL = 20%, WIND SPEED = 7 m/s, AND SG_2 TRIP = 100 MW

Fig. 13 shows the results for Case 4 and Case 5, which are the same as Case 2 except for the size of an event. For 'w/o WPP' in Case 4, the frequency is stabilized at 59.507 Hz 16.0 s after the event and then is restored to f_0 (see Fig. 13(a)). After the event, β in Case 4 with a WPP is 15 MW/0.1 Hz, as in the previous cases. The size of the event is 100 MW, which is 10 MW larger than it is in the previous cases. In addition, the load consumption is changed from 287.2 MW to 271.9 MW. Thus, the frequency is stabilized at 59.408 Hz 21.8 s after the event (see Figs. 13(b) and 13(c)), which is 0.069 Hz less than it is in Case 2.

As in the previous cases, the proposed scheme starts at 70.0 s. The output power of the DFIG is instantly increased by 0.750 MW (see Fig. 13(d)), and thus P_e is reduced by 0.750 MW while maintaining P_{gov}. The frequency increases at the rate of 20 mHz/s. The output power of the DFIG returns to its original value at 79.4 s. It takes more time to reach 59.6 Hz than it does in Case 2 because f_{set} is lower. During this interval, the DFIG releases more energy than it does in Case 2, and thus the rotor speed decreases from 0.790 p.u. to 0.774 p.u. (see Fig. 13(e)). This is because the DFIG releases energy for a longer time than it does in Case 2.

2) CASE 5: WIND PENETRATION LEVEL = 20%, WIND SPEED = 7 m/s, AND SG_2 TRIP = 110 MW

For 'w/o WPP' in Case 5, the frequency is stabilized at 59.483 Hz 20.2 s after the event but is not restored to f_0 (see Fig. 13(a)). The frequency in Case 5 with a WPP is stabilized at 59.340 Hz 22.4 s after the event, which is less than in Case 4 by 0.068 Hz. This is because the event is 10 MW larger than in Case 4 though β and the load reduction are the same.

The DFIG instantly increases its output power by 0.750 MW at 70.0 s and decreases at 82.6 s (see Fig. 13(d)). It takes more time to reach 59.6 Hz than it does in Case 2 and Case 4 because f_{set} is lower. In this case, the DFIG releases more energy, and thus the rotor speed decreases to 0.768 p.u., which is 0.006 p.u. less than in Case 4 (see Fig. 13(e)).

The results in Case 4 and Case 5 clearly demonstrate that the proposed scheme successfully increases the frequency, even for the larger events, so that AGC can be activated.

D. EFFECTS OF WIND PENETRATION LEVELS

The performance of the proposed scheme depends on the wind penetration level. As the wind penetration level increases, β decreases, thereby further reducing the settling frequency. Thus, this subsection describes the investigation results with the wind penetration level of 60%.

1) CASE 6: WIND PENETRATION LEVEL = 60%, WIND SPEED = 7 m/s, AND SG_2 TRIP = 110 MW

Fig. 14 shows the results for Case 6, which is the same as Case 5 except for the wind penetration level of 60%. In this case, to simulate the wind penetration of 60%, SG_3 and SG_4 are out of service, and the installed capacity of the WPP increases from 60 MW to 180 MW (see Table 4). After the event, β is decreased from 15 MW/0.1 Hz to 9.5 MW/0.1 Hz, which is smaller than the previous cases by 5.5 MW/0.1 Hz (see Table 6). In addition, the load consumption is decreased from 276.6 MW to 237.7 MW. Thus, f_{set} is 59.208 Hz

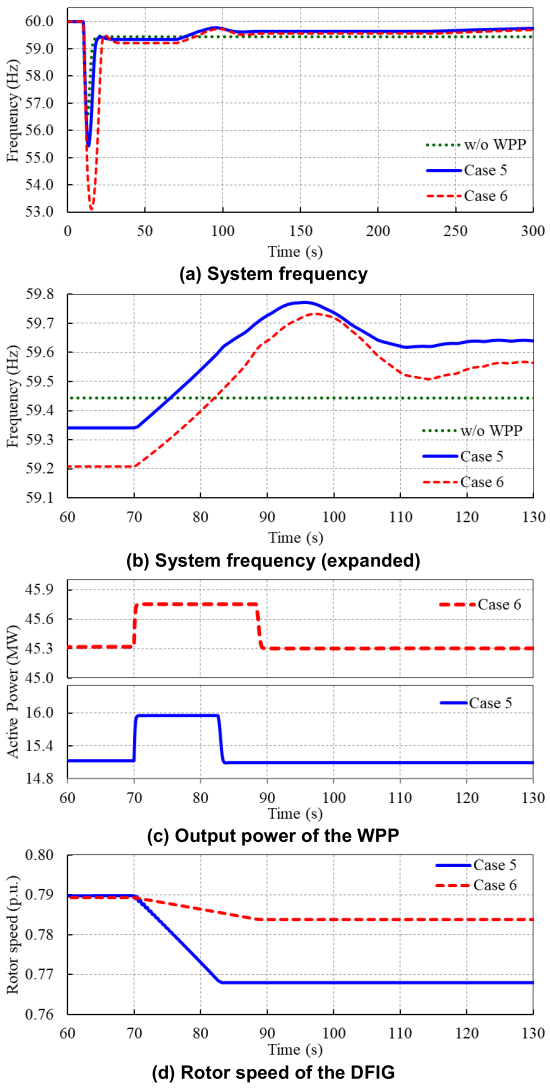

FIGURE 14. Results for Case 6.

TABLE 6. Summary of numerical results for the six cases.

	Case 1	Case 2	Case 3	Case 4	Case 5	Case 6
β (MW/0.1 Hz)	15	15	15	15	15	9.5
f_{set} (Hz)	59.475	59.477	59.473	59.408	59.340	59.208
ΔP (MW)	0.750	0.750	0.750	0.750	0.750	0.432
Time to f_{mssd} (s)	1.391	1.352	1.408	4.667	7.892	14.452
Released energy (s)	0.081	0.080	0.081	0.125	0.171	0.047

at 28.1 s, which is less than it is in Case 5 by 0.132 Hz (see Figs. 14(a) and 14(b)).

In the proposed scheme, the DFIG instantly increases its output power by 0.432 MW, which is smaller than it is in Case 5 by 0.318 MW, at 70.0 s (see Fig. 14(c)). This is because J in (1) in Case 6 is smaller than in the previous cases because of the reduced number and installed capacity of the synchronous generators; as a result, the required ΔP to increase the frequency at the rate of 20 mHz/s is smaller (refer to (1)). When the frequency reaches 59.6 Hz at 88.3 s, the DFIG instantly reduces its output to the original value. It takes more time, 5.7 s, to reach 59.6 Hz than it does in Case 5 because f_{set} is lower. During this interval, the rotor speed decreases by 0.006 p.u., from 0.789 p.u. to 0.783 p.u. (see Fig. 14(d)); this value is higher than it is in Case 5. This is because a higher wind penetration level indicates that a power grid has more releasable energy, and thus less energy is released from the DFIG for an event of the same size.

Table 6 summarizes the numerical results for the six cases in this paper in terms of β after the event, f_{set}, ΔP, time to f_{mssd}, and normalized released energy. From the case studies, it is proved that the proposed scheme successfully increases the settling frequency at a low wind speed even with a severe event for AGC activation. Further, in a higher wind penetration level, the proposed scheme can release less energy from DFIG to increase the settling frequency.

VI. CONCLUSION

This paper proposes a frequency stability support scheme for a DFIG to improve the settling frequency in association with the control of synchronous generators. In the proposed scheme, if the frequency is stabilized at a value beyond the maximum SSFD band, a DFIG instantly increases the output power by a constant and maintains this value until the frequency increases to within the maximum SSFD band. At the same time, the mechanical input power of synchronous generators is maintained so that the difference between the input power and output power of the synchronous generators can increase the frequency.

The various simulation results clearly demonstrate that the proposed scheme is able to improve the settling frequency for AGC activation when the frequency is stabilized to a value beyond the maximum SSFD band while avoiding additional system defense plans under various scenarios, such as wind speed, event size, and wind penetration level. The advantages of the proposed scheme are that it enables to support PFC by improving the settling frequency for AGC activation without additional system defense plans. In addition, for higher wind penetration levels, part of WTGs can be used to improve the settling frequency while SIC schemes can be implemented in the rest of WTGs depending on grid conditions. Therefore, the scheme helps provide a promising solution to ancillary services, such as supporting PFC in a power grid that has high penetrations of VRE. However, to successfully participate in improving the settling frequency, WTGs should keep the minimum kinetic energy to be released. In addition, the proposed scheme requires a monitoring system of the available kinetic energy in a grid level that can be released to improve the settling frequency. Further, the control parameters suitable for various system conditions and event sizes should be set through comprehensive studies.

REFERENCES

[1] J. Machowski, J. W. Bialek, and J. R. Bumby, "Frequency stability and control," in *Power System Dynamics: Stability and Control*, 2nd ed. Warminster, U.K.: Wiley, 2008.

[2] F. Díaz-González, M. Hau, A. Sumper, and O. Gomis-Bellmunt, "Participation of wind power plants in system frequency control: Review of grid code requirements and control methods," *Renew. Sustain. Energy Rev.*, vol. 34, pp. 551–564, Jun. 2014.

[3] J. Undrill, "Power and frequency control as it relates to wind-powered generation," Lawrence Berkley Nat. Lab., Berkeley, CA, USA, Tech. Rep. LBNL-4143E, Dec. 2010.
[4] *Getting Wind and Sun on to the Grid—A Manual for Policy Makers*, Int. Energy Agency, Paris, France, 2017.
[5] *Establishing a Network Code on Requirements for Grid Connection of Generators*, document Commission regulation (EU) 2016/631, ENTSO-E, Apr. 2016.
[6] *IGD on Need for Synthetic Inertia for Frequency Regulation*, ENTSO-E, Brussels, Belgium, Mar. 2017.
[7] J. Morren, S. De Haan, W. Kling, and J. Ferreira, "Wind turbines emulating inertia and supporting primary frequency control," *IEEE Trans. Power Syst.*, vol. 21, no. 1, pp. 433–434, Feb. 2006.
[8] M. Kayikci and J. Milanovic, "Dynamic contribution of DFIG-based wind plants to system frequency disturbances," *IEEE Trans. Power Syst.*, vol. 24, no. 2, pp. 859–867, May 2009.
[9] Z.-S. Zhang, Y.-Z. Sun, J. Lin, and G.-J. Li, "Coordinated frequency regulation by doubly fed induction generator-based wind power plants," *IET Renew. Power Gener.*, vol. 6, no. 1, pp. 38–47, Jan. 2012.
[10] T. Liu, W. Pan, R. Quan, and M. Liu, "A variable droop frequency control strategy for wind farms that considers optimal rotor kinetic energy," *IEEE Access*, vol. 7, pp. 68636–68645, 2019.
[11] X. Zeng, T. Liu, S. Wang, Y. Dong, and Z. Chen, "Comprehensive coordinated control strategy of PMSG-based wind turbine for providing frequency regulation services," *IEEE Access*, vol. 7, pp. 63944–63953, 2019.
[12] M. Hwang, E. Muljadi, G. Jang, and Y. C. Kang, "Disturbance-adaptive short-term frequency support of a DFIG associated with the variable gain based on the ROCOF and rotor speed," *IEEE Trans. Power Syst.*, vol. 32, no. 3, pp. 1873–1881, May 2017.
[13] N. Ullah, T. Thiringer, and D. Karlsson, "Temporary primary frequency control support by variable speed wind turbines-potential and applications," *IEEE Trans. Power Syst.*, vol. 23, no. 2, pp. 601–612, May 2008.
[14] M. Kang, K. Kim, E. Muljadi, J.-W. Park, and Y. C. Kang, "Frequency control support of a doubly-fed induction generator based on the torque limit," *IEEE Trans. Power Syst.*, vol. 31, no. 6, pp. 4575–4583, Nov. 2016.
[15] D. Yang, J. Kim, Y. C. Kang, E. Muljadi, N. Zhang, J. Hong, S.-H. Song, and T. Zheng, "Temporary frequency support of a DFIG for high wind power penetration," *IEEE Trans. Power Syst.*, vol. 33, no. 3, pp. 3428–3437, May 2018.
[16] *Reliability Guideline: Primary Frequency Control*, North Amer. Electr. Rel. Corp., Atlanta, GA, USA, 2015.
[17] J. H. Eto, J. Undrill, P. Mackin, R. Daschmans, B. Williams, B. Haney, R. Hunt, J. Ellis, H. Illian, C. Martinez, M. O'Malley, K. Coughlin, and K. H. LaCommare, "Use of frequency response metrics to assess the planning and operating requirements for reliable integration of variable renewable generation," Lawrence Berkeley Nat. Lab., Berkeley, CA, USA, Tech. Rep. LBNL-4142E, Dec. 2010.
[18] B. Boukhezzar and H. Siguerdidjane, "Nonlinear control of a variable-speed wind turbine using a two-mass model," *IEEE Trans. Energy Convers.*, vol. 26, no. 1, pp. 149–162, Mar. 2011.
[19] E. Muljadi and C. Butterfield, "Pitch-controlled variable-speed wind turbine generation," *IEEE Trans. Ind. Appl.*, vol. 37, no. 1, pp. 240–246, Jan. 2001.
[20] IEEE Committee Report, "Dynamic models for steam and hydro turbines in power system studies," *IEEE Trans. Power App. Syst.*, vol. PAS-92, no. 6, pp. 1904–1915, Nov. 1973.
[21] P. Kundur, *Power System Stability and Control*. New York, NY, USA: McGraw-Hill, 1994.
[22] H. Holttinen, "Overview of integration studies—Methodologies and results," in *Wind Power in Power System*, 2nd ed. Hoboken, NJ, USA: Wiley, 2012.

JAE IK YOO (Student Member, IEEE) received the B.S. and Ph.D. degrees from the School of Electrical and Electronic Engineering, Yonsei University, Seoul, South Korea, in 2012 and 2020, respectively. He is currently working with Hyundai Heavy Industry company. His research interests include the frequency stability of power systems, control of wind turbine systems, and renewable energy-based distributed generation systems.

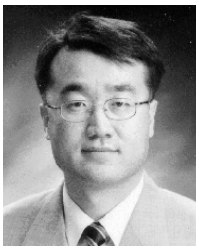

YONG CHEOL KANG (Senior Member, IEEE) received the B.S., M.S., and Ph.D. degrees in electrical engineering from Seoul National University, South Korea, in 1991, 1993, and 1997, respectively. From 1999 to 2017, he was a Professor with the Department of Electrical Engineering, Chonbuk National University, Jeonju, South Korea. He was the Director of the WeGAT Research Center supported by the MSIP, South Korea. Since 2018, he has been with Yonsei University, Seoul. His research interest includes the development of control and protection techniques for wind power plants. He is a member of the International Electrotechnical Commission Working Group TC88/WG27 and an Editor of the IEEE TRANSACTIONS ON SUSTAINABLE ENERGY.

EDUARD MULJADI (Fellow, IEEE) received the Ph.D. degree in electrical engineering from the University of Wisconsin–Madison. From 1992 to 2017, he was with the National Renewable Energy Laboratory, Golden, CO, USA. Since 2018, he has been a James J. Danaher Distinguished Professor with the Department of Electrical and Computer Engineering, Auburn University, Auburn, AL, USA. His current research interests are in the fields of electric machines, power electronics, and power systems in general, with an emphasis on renewable energy applications. He is involved in the activities of the IEEE Industry Application Society, the Power Electronics Society, and the Power and Energy Society (PES). He is an Editor of the IEEE TRANSACTIONS ON ENERGY CONVERSION.

KYU-HO KIM (Member, IEEE) received the B.S., M.S., and Ph.D. degrees from Hanyang University, South Korea, in 1988, 1990, and 1996, respectively. He is currently a Professor with the Department of Electrical, Electronic, and Control Engineering, Hankyong National University, South Korea. His research interests include power system control and operation, optimal power flow, and renewable energy systems.

JUNG-WOOK PARK (Senior Member, IEEE) was born in Seoul, South Korea. He received the B.S. degree *(summa cum laude)* from the Department of Electrical Engineering, Yonsei University, Seoul, in 1999, and the M.S.E.C.E. and Ph.D. degrees from the School of Electrical and Computer Engineering, Georgia Institute of Technology, Atlanta, GA, USA, in 2000 and 2003, respectively. From 2003 to 2004, he was a Postdoctoral Research Associate with the Department of Electrical and Computer Engineering, University of Wisconsin–Madison, Madison, WI, USA, and a Senior Research Engineer with LG Electronics Inc., South Korea, from 2004 to 2005. Since 2005, he has been with the School of Electrical and Electronic Engineering, Yonsei University, where he is currently a Professor. His current research interests include power system dynamics, energy management systems, renewable energy-based distributed generation systems, operation and planning of microgrid, and hardware implementation of power-electronic-based inverters.